

# The importance of turbulent ocean-sea ice nutrient exchanges for simulation of ice algal biomass and production with CICE6.1 and Icepack 1.2

Pedro Duarte<sup>1</sup>, Philipp Assmy<sup>1</sup>, Karley Campbell<sup>2,3</sup>, Arild Sundfjord<sup>1</sup>

<sup>1</sup> Norwegian Polar Institute, Fram Centre, Tromsø, Norway

<sup>2</sup> Department of Arctic and Marine Biology, UiT The Arctic University of Norway, Norway

<sup>3</sup> Bristol Glaciology Centre, University of Bristol, UK

*Correspondence to:* Pedro Duarte (Pedro.Duarte@npolar.no)

**Abstract.** Different sea-ice models apply unique approaches in the computation of nutrient diffusion between the ocean and the ice bottom, which are generally decoupled from the calculation of turbulent momentum and heat flux. Often, a simple molecular diffusion formulation is used. We argue that nutrient transfer from the ocean to sea ice should be as consistent as possible with momentum and heat transfer, since all these fluxes respond to varying forcing in a similar fashion. We hypothesize that biogeochemical models which do not consider such turbulent nutrient exchanges between the ocean and the sea-ice, ~~despite considering brine drainage and bulk exchanges through ice freezing/melting, may~~ underestimate bottom-ice algal production. The Los Alamos Sea Ice Model (CICE + Icepack) was used to test this hypothesis by comparing simulations ~~without and with molecular and turbulent~~ diffusion of nutrients ~~across sea-ice bottom dependent on velocity-shear into the bottom of sea-ice~~, implemented in a way that is consistent with turbulent momentum and heat exchanges. Simulation results support the hypothesis, showing a significant enhancement of ice algal production and biomass when nutrient limitation was relieved by bottom-ice turbulent exchange. Our results emphasize the potentially critical role of turbulent exchanges to sea ice algal blooms, and the importance of thus properly representing them in biogeochemical models. The relevance of this becomes even more apparent considering ongoing trends in the Arctic Ocean, with a predictable shift from light to nutrient limited growth of ice algae earlier in the spring, as the sea ice becomes more fractured and thinner with a larger fraction of young ice with thin snow cover.

## 1 Introduction

Momentum, heat and mass fluxes between the ocean and the sea-ice are of utmost importance to predict sea-ice motion, thermodynamics, and biogeochemistry. Considering the interlinks between these processes one would expect that sea-ice models used a common approach to compute them, notwithstanding their obvious specificities. However, when we look at models ~~published-released~~ over the last decades, we find not only inter-model differences in the physical concepts used to describe the processes responsible for some of the above fluxes, but also intra-model differences in the approaches used in

31 calculating, for example, heat and mass fluxes. In this work we will focus on the differences related with the vertical diffusion  
32 of tracers between the water column and the bottom-ice and attempt to explore their consequences on nutrient limitation for  
33 sea-ice algal growth.

34 The most common processes found in the literature to model nutrient exchanges between the water and the sea ice are based  
35 on entrapment during freezing, release during melting and ~~brine transport diffusive or convective fluxes~~ (e.g. Arrigo et al.,  
36 1993; Jin et al., 2006; Tedesco and Vichi, 2010; Jeffery et al., 2011; [Vancoppenolle et al., 2013](#)). Arrigo et al. (1993)  
37 distinguished nutrient exchanges resulting from gravity drainage in brine channels, from brine convection in the skeletal layer,  
38 dependent on the ice growth rate. These brine fluxes were used to calculate nutrient exchanges as a diffusive process. Lavoie  
39 et al. (2005) also calculated nutrient exchanges as a diffusive process. Jin et al. (2006; 2008) computed nutrient fluxes across  
40 the bottom layer as an advection process dependent on ice growth rate and based on Wakatsuchi and Ono (1983). Molecular  
41 diffusion was also considered. More recently, other authors have integrated formulations of “enhanced diffusion”  
42 ([Vancoppenolle et al., 2010](#); [Jeffery et al., 2011](#)) or convection ([Turner et al., 2013](#)), based on hydrostatic instability of brine  
43 density profiles, to compute brine gravity drainage and tracer exchange within the ice and between the ice and the sea water;  
44 ~~based on diffusive~~ ([Vancoppenolle et al., 2010](#); [Jeffery et al., 2011](#)) or ~~convective processes~~ ([Turner et al., 2013](#)). Comparisons  
45 between salt dynamics in growing sea ice with salinity measurements showed that convective Rayleigh number-based  
46 parameterizations (e.g. Wells et al., 2011), such as the one by Turner et al. (2013), outperform diffusive and simple convective  
47 formulations (Thomas et al., 2020).

48 Interestingly, the ~~resulting~~ calculation of momentum and heat exchange versus salinity in models is often mismatched. In the  
49 case of the former two, typically, a transfer mechanism (turbulent or not) at the interface between the ocean and the sea ice is  
50 not dependent on any type of brine exchange. In the case of salinity, such a mechanism is not considered (e.g. Vancoppenolle  
51 et al., 2007; Turner et al., 2013). Presumably, such differences result from the relative importance of various physical processes  
52 for different tracers. Momentum and heat transfer between the ice and the water are fundamental mechanisms in explaining  
53 sea-ice dynamics and thermodynamics, irrespective of brine exchanges. However, ice desalination depends mostly on brine  
54 gravity drainage and flushing during melting (Notz and Worster, 2009).

55 Vertical convective mixing of nutrients under the sea ice may result from brine rejection and/or drainage from the sea ice (Lake  
56 and Lewis, 1970; Niedrauer and Martin, 1979; Reeburgh, 1984) and from turbulence due to shear instabilities generated by  
57 drag at the ~~ice-ocean~~ interface between the ocean and the sea ice ([Gosselin et al., 1985](#); [Cota et al., 1987](#); [Carmack, 1986](#)),  
58 internal waves and topographical features ([Ingram et al., 1989](#); [Dalman et al., 2019](#)). [Gosselin et al. \(1985\)](#) and [Cota et al.](#)  
59 [\(1987\)](#) stressed the significance of tidally induced mixing in supplying nutrients to sympagic algae. Biological demand for  
60 silicic acid (hereafter abbreviated as silicate) and nitrate is limited by the physical supply ([Cota and Horne, 1989](#); [Cota and](#)  
61 [Sullivan, 1990](#)). Vertical nutrient fluxes between the water and the bottom ice can be calculated from:

$$62 \quad F_c = -K_z K_z \frac{\Delta C}{\Delta z},$$

63 (1)

Formatted: Font: (Default) Times New Roman, Not Italic

64 where  $K_z$  is the vertical eddy diffusivity ( $\text{m}^2 \text{d}^{-1}$ ) and  $\Delta C$  is the difference in nutrient concentration ( $\text{mmol m}^{-3}$ ) over the vertical  
65 distance  $\Delta z$  ( $\text{mmol m}^{-1} \text{m}$ ) (Cota et al., 1987).

66 ~~Even though this eddy diffusion approach was proposed more than 30 years ago, it has been rarely used in the literature.~~ Table  
67 1 summarizes several models published over the last decades and their approaches to ~~the calculation of~~ calculate nutrient-tracer  
68 diffusion ~~between the ocean and bottom ice~~. Some models do not consider this process ~~or~~ and-limit nutrient-itexchanges to  
69 ~~brine molecular diffusion dynamics and/or entrapment during freezing and release during melting~~. Other models consider  
70 ~~turbulent exchanges parameterized as a function of the Rayleigh number, calculated from brine vertical density gradients~~. Only  
71 one of the sampled models (Mortenson et al., 2017) uses a parameterization based on friction velocity, ~~whereas the others~~  
72 ~~either do not consider nutrient diffusion or use molecular diffusion~~.

73 From this assessment one may divide the ocean-ice exchange processes of existing biogeochemical models into those related  
74 to: (i) entrapment during freezing; ~~(ii) brine drainage, driven by density instability;~~(ii) flushing and release during melting; (iii)  
75 ~~brine gravity drainage, driven by density instability, parameterized as either a diffusive or a convective process; flushing,~~  
76 ~~driven by snow and ice melting, and~~ (iv) ~~molecular diffusive-diffusionexchanges;~~ (v) turbulent diffusion at the interface  
77 between the ocean and the ice ~~induced by velocity shear, dependent on concentration gradients – the focus of this study~~. In the  
78 absence of ice growth and when brine ~~gravity~~ drainage is limited, diffusive nutrient exchanges between the ocean and the ice  
79 have the capacity to limit primary production. This limitation will be alleviated in the presence of a turbulent exchange  
80 mechanism. We argue that nutrient transfer ~~at the interface between the ocean and the sea ice~~ should be as consistent as possible  
81 with momentum and heat transfer since all these fluxes are closely linked. We hypothesize that models which do not consider  
82 ~~the role of current velocity shear on~~ turbulent nutrient exchanges between the ocean and the sea-ice may underestimate bottom-  
83 ice ~~ice~~-algal production. Such underestimation will bias the role of sea ice algae in ice associated food webs and ecosystem  
84 services, such ~~as~~ carbon dioxide exchanges and their climate feedbacks.

85 To test the above hypothesis, we use a 1D vertically resolved model and contrast results using the default ~~molecular~~-diffusion  
86 parameterization and a “turbulent” parameterization analogous to that of momentum and heat transfer, ~~at the interface between~~  
87 ~~the ocean and the sea ice~~, based on McPhee (2008).

89 **Table 1. Model parameterizations used/proposed by different authors to compute diffusion of nutrientstracers at the ice-ocean**  
90 **interface, independent of brine exchanges and/or ice growth/melting. The only example based on friction velocity is that of**  
91 **Mortenson et al. (2017). “None” is used when exchange processes depend solely on brine exchanges and/or ice growth/melting.**

Source	Type of diffusion	Associated model
Cota et al. (1987)	Eddy diffusion	-
Arrigo et al. (1993)	<del>None</del> Diffusion based on brine fluxes	A simulated Antarctic fast ice ecosystem
Lavoie et al. (2005)	Molecular diffusion ( $1 \times 10^{-9} \text{ m}^2 \text{ s}^{-1}$ )	Ice algal modelling of the Arctic in Resolute Passage, Canadian archipelago.
Jin et al. (2006; 2008)	Molecular diffusion according to the authors but using a diffusion coefficient ( $1.0 \times 10^{-5} \text{ m}^2 \text{ s}^{-1}$ ) that is 4 orders of	Ice-ocean ecosystem model for 1-D and 3-D applications in the Bering and Chukchi seas.

Formatted: Superscript

Formatted: Tab stops: 0.94", Left

	magnitude higher than molecular diffusion of salt [ $1.0 \times 10^{-9} \text{ m}^2 \text{ s}^{-1}$ , following Mann and Lazier (2005)]	
Tedesco and Vichi (2010 and e.g. 2019)	None	Biogeochemical flux model in sea ice
Vancoppenolle et al. (2010)	None	Modelling brine and nutrient dynamics in Antarctic sea ice
Mortenson et al. (2017)	Diffusion parameterized as a function of friction velocity	Biogeochemical model representing the low trophic levels of sea ice and pelagic ecosystems in the Arctic.
Jeffery et al. (2011)	Diffusion parameterized as a function of the Rayleigh number	Los Alamos Sea Ice Model
Mortenson et al. (2017) Hunke et al. (2016)	Diffusion parameterized as a function of friction velocity	Biogeochemical model representing the low trophic levels of sea ice and pelagic ecosystems in the Arctic.
	Molecular diffusion	Los Alamos Sea Ice Model

Formatted: Portuguese (Portugal)

## 2 Methods

### 2.1 Concepts

Eq. (1) from Cota et al. (1987) provides the basis for our reasoning about nutrient exchanges between the ocean and the sea-ice bottom being based on a turbulent exchange process enhanced by current velocity shear, irrespective of other exchanges based on brine dynamics, ice melt and ice growth. These turbulent exchanges may be parameterized through the flux of a quantity at the ocean-ice interface between the ocean and the sea ice, calculated as the product of a scale velocity and the change in the quantity from the boundary to some reference level (McPhee, 2008):

$$\langle w' S' \rangle = \alpha_s \alpha_s u^* (S_w - S_0) \quad (2)$$

Where,  $w'$  and  $S'$  are interface vertical velocity ( $\text{m s}^{-1}$ ) and salinity, respectively,  $\alpha_s$  is an interface salt/nutrient exchange coefficient (dimensionless);  $u^*$  is the friction velocity ( $\text{m s}^{-1}$ );  $S_0$  and  $S_w$  are sea-ice-interface and far-field salinities, respectively.

Hereafter we will assume that salt turbulent exchanges are similar to nutrient exchanges and governed by the same principles and parameters. The main difference between turbulent heat and salt/nutrient exchanges is due to the exchange coefficients that may be higher for heat. The heat exchange coefficient ( $\alpha_h$ ) is around 0.006. The ratio ( $R$ ) between  $\alpha_h$  and  $\alpha_s$  may vary from unity to a range between 35 and 70 during ice melting and because of double diffusion, leading to a range in  $\alpha_s$  between 8.6  $10^5$  and 0.006 (McPhee et al., 2008).

The net downward heat flux from the ice to the ocean in the Los Alamos Sea Ice Model (CICE + Icepack) is given by (Hunke et al., 2015) and it is computed according to MCPhee et al. (2008) [Eq. (2)]:

$$F_{bot} = -\rho_w c_w \alpha_h u^* (T_w - T_f) \quad (3)$$

Formatted: Font: Italic

Formatted: Font: Italic

Formatted: Font: Not Italic, Not Superscript/ Subscript

Formatted: Superscript

Where,  $\rho_w$  is the density of seawater ( $\text{kg m}^{-3}$ );  $c_w$  is the specific heat of seawater ( $\text{J kg}^{-1} \text{K}^{-1}$ );  $\alpha_h$  is the heat transfer coefficient (dimensionless);  $T_w$  is the water temperature (K);  $T_f$  if the freezing temperature (K).

$$[W m^{-2}] = [kg m^{-3}] [J kg^{-1} K^{-1}] [dimensionless] [m s^{-1}] [K]$$

We calculate salt or nutrient exchanges using a similar approach:

$$F_N = -\alpha_s u^* (N_w - N_i) \quad (4)$$

In fact, this agrees with McPhee (2008) (see page 112, Fig. 6.3). The minus sign used in (3) and (4) is for compatibility with the CICE + Icepack convention that upward fluxes are negative (e.g. Hunke et al., 2015).

$$[g m^{-2} s^{-1}] = [dimensionless] [m s^{-1}] [g m^{-2}]$$

A timescale for this turbulent process may be calculated from:

$$\tau = \frac{\alpha_s u^*}{H} [s^{-1}] \quad (5)$$

Where  $H$  is the vertical distance over which diffusion is to be calculated (m). In the Los Alamos Sea Ice Model, it corresponds to the layer thickness of the biogeochemical grid (biogrid), used for discretizing the vertical transport equations of biogeochemical tracers and defined between the ice bottom and the brine height (Jeffery et al., 2017, 2016). The above time scale is calculated for consistency with CICE implementation of diffusion, where a comparable time scale is calculated as:

$$\tau = \frac{D_m D_m}{H^2} [s^{-1}] \quad (6)$$

Or

$$\tau = \frac{D_{MLD}}{h^2} [s^{-1}] \quad (7)$$

Where  $D_m$  is the molecular diffusion coefficient and  $D_{MLD}$  is the mixed length diffusion coefficient ( $\text{m}^2 \text{s}^{-1}$ ) (Jeffery et al., 2011).

Eq. (5) or (6) These time scales expressed in equations 6 and 7 are included in must be multiplied by ice porosity and then used to compute matrix coefficients for the Icepack transport equation, which may be written as [for more details, refer Jeffery et al. (2011)]:

$$\text{along the biogrid (Hunke et al., 2016). } \varphi \frac{\partial N}{\partial t} = \left\{ \frac{(x-1)}{h} \frac{\partial z_t}{\partial t} - \frac{x}{h} \frac{\partial z_b}{\partial t} \right\} \frac{\partial}{\partial x} (\varphi N) + \frac{1}{h} \frac{\partial}{\partial x} (w_f N) + \frac{\partial}{\partial x} \left( \frac{D_{MLD} + \varphi D_m}{h^2} \frac{\partial N}{\partial x} \right) \quad (8)$$

Where  $0 \leq x \leq 1$  is the relative depth of the vertical domain of the biogrid,  $z_a$  and  $z_b$  are vertical distances from the interface between the ocean the sea ice (m).  $\varphi$  is sea ice porosity,  $w_f$  is the Darcy velocity due to the sea ice flushing of tracers ( $\text{m s}^{-1}$ ).

$D_{MLD}$  is detailed in Jeffery et al. (2011) and it is zero when the brine vertical density gradient is stable, otherwise (when density increases towards the ice top) it is calculated as:

$$D_{MLD} = \frac{gk}{\mu} \Delta \rho_e l \quad (9)$$

Where  $g$  is the acceleration of gravity ( $9.8 \text{ m s}^{-2}$ ),  $k$  is sea ice permeability,  $\mu$  is dynamic viscosity ( $2.2 \text{ kg m}^{-1} \text{s}^{-1}$ ),  $\rho_e$  is the equilibrium brine density and  $l$  is a length scale (7 m). The values shown here are the default ones in Icepack.

We rewrite the last term of 7 for the bottom ice layer as:

- Formatted: Subscript
- Formatted: Superscript
- Formatted: Superscript
- Formatted: Font: Italic
- Formatted: Font: Not Italic
- Formatted: Font: Italic, Subscript
- Formatted: Font: Italic
- Formatted: Font: Italic, Subscript
- Formatted: Font: Italic, Subscript
- Formatted: Superscript
- Formatted: Font: Italic
- Formatted: Superscript
- Formatted: Font: Italic
- Formatted: Font: Symbol, Italic
- Formatted: Superscript
- Formatted: Superscript
- Formatted: Font: Symbol, Italic
- Formatted: Font: Italic, Subscript
- Formatted: Not Superscript/ Subscript
- Formatted: Font: Italic

$$\varphi \frac{\partial N}{\partial t} = \left\{ \frac{(x-1)}{h} \frac{\partial z_t}{\partial t} - \frac{x}{h} \frac{\partial z_b}{\partial t} \right\} \frac{\partial}{\partial x} (\varphi N) + \frac{1}{h} \frac{\partial}{\partial x} (w_f N) + \frac{\partial}{\partial x} \left( \frac{\alpha_s u^*}{h} \frac{\partial N}{\partial x} \right) \quad (10)$$

The transport equation is resolved along the biogrid, with a Flux-Corrected, Positive Definite Transport Scheme, using the finite element Galerkin discretization (Jeffery et al., 2016).

Therefore, the implementation of turbulent diffusion nutrient exchanges in terms consistent with momentum and heat exchanges is quite straightforward in the CICE model, depending on changing the timescales from Eq. (6) or (7) to (5). In other models, other approaches may be required.

From equations 5 - 7 it turns out that the product  $\alpha_s u^* h$  has the same dimensions of  $D_w$  or  $D_{MLD}$ , corresponding to a turbulent diffusion coefficient. Assuming  $h \approx 0.01$  m, turbulent diffusion induced by velocity shear, becomes comparable with molecular diffusion only for  $u^* < 0.0012$  m s<sup>-1</sup>, considering the lower end of the  $\alpha_s$  range ( $8.6 \cdot 10^{-5}$ , see above) or  $u^* < 1.7 \cdot 10^{-5}$  m s<sup>-1</sup>, considering the upper end of the  $\alpha_s$  range (0.006). If we assume instead  $h \approx 0.001$  m, the calculated  $u^*$  values become one order of magnitude higher but still very low. In fact, such low friction velocities would require extremely low “stream” velocities - relative ice-ocean velocities. For an account of the relationship between “stream” and friction velocities under the sea ice see Supplementary information 3 of Olsen et al. (2019) and references therein. These authors show that “stream” velocities of only a few centimetres per second lead to friction velocities one order of magnitude lower but still in the order of 0.001 ms<sup>-1</sup>, i.e., comparable only to the highest  $u^*$  estimated above. Considering current velocities relative to the sea ice observed during the N-ICE2015 cruise (Granskog et al., 2018; Figure 2d of Duarte et al., 2017), with most values between 0.05 and > 0.2 m s<sup>-1</sup>, it is rather likely that friction velocities under the ice are frequently above the thresholds calculated above and that turbulent diffusion will dominate over molecular diffusion. Dalman et al. (2019) provided experimental evidence for such turbulent nutrient fluxes to the ice bottom, leading to increased chlorophyll concentrations at the bottom ice, in a strait with strong tidal currents. The mechanism treated here as turbulent diffusion seems analogous to “forced convection” in the lowermost parts of the brine network, which is driven by pressure differences caused by the shear under the sea ice (Neufeld, 2008; Vancoppenolle et al., 2013).

## 2.2 Implementation

We used the Los Alamos Sea Ice Model, which is managed by the CICE Consortium with an active forum (<https://bb.cgd.ucar.edu/cesm/forums/cice-consortium.146/>) and a git repository (<https://github.com/CICE-Consortium>). It includes two independent packages: CICE and Icepack. The former computes ice dynamic processes and the latter ice column physics and biogeochemistry. Their development is handled independently with respect to the GitHub repositories (<https://github.com/CICE-Consortium>). All the changes described below were implemented in two forks to the above repository, one for Icepack and another for CICE and they may be found in Duarte (2021a and b, respectively).

Our simulations may be run using only Icepack, since they are focused on ice column physics and biogeochemistry, without the need to consider ice dynamic processes. However, we used both CICE + Icepack together to allow for use of netCDF based input/output not included in Icepack. Therefore, we defined a 1D vertically resolved model with 1 snow layer and 15 ice layers

Formatted: Font: Italic

Formatted: Font: Italic

Formatted: Font: Italic, Subscript

Formatted: Subscript

Formatted: Font: Not Italic

Formatted: Superscript

Formatted: Font: Italic

Formatted: Superscript

Formatted: Font: Italic

Formatted: Superscript

176 and 5X5 horizontal cells. This is the minimum number of cells allowable in CICE due to the need to include halo cells (only  
177 the central “column” is simulated). Therefore, ice column physics and biogeochemistry were calculated by Icepack but CICE  
178 was the model driver. The input file (ice\_in) used in this study was included in our CICE fork and it lists all parameters used  
179 in the model and described in Hunke et al. (2016), Jeffery et al. (2016), Duarte et al. (2017) and in Tables S1 and S2. Any  
180 changes in “default” parameters or any other model settings will be specified.

181 We made several modifications in CICE to allow using forcing time series collected during the Norwegian Young Sea Ice  
182 Expedition (N-ICE2015) (Granskog et al., 2018) and described in Duarte et al. (2017) (see Fig. 2 of the cited authors). These  
183 modifications were meant to allow reading of forcing data at higher frequencies than possible with the standard input  
184 subroutines in the CICE file ice\_forcing.F90.

185 When the dynamical component of CICE is not used,  $u^*$  is set to a minimum value instead of being calculated as a function of  
186 ice-ocean shear stress (Hunke et al., 2015). Duarte et al. (2017) implemented shear calculations from surface current velocities  
187 (one of the models forcing functions) irrespective of using or not the CICE dynamics code. These modifications were also  
188 incorporated in the current model configuration so that shear can be used to calculate friction velocity and, thereafter, influence  
189 heat and tracer/nutrient exchanges, following Eqs. (3) and (4) and parameters described in McPhee et al. (2008). When the  
190 parameter `kdyn` is set to zero in `ice_in`, ice dynamics is not computed, but shear is calculated in the modified subroutine  
191 `icepack_step_therm1`, file `icepack_therm_vertical.F90`. If `kdyn` is not zero, these calculations are ignored since shear is already  
192 calculated in the dynamical part of the CICE code.

193 A Boolean parameter (`Bottom_turb_mix`) was added to the input file, which is set to “false” or “true” when the standard  
194 molecular diffusion approach or the new turbulent based diffusion approach is to be used, respectively. Another Boolean  
195 (`Limiting_factors_file`) was added to the `ice_in` file. When set to “true” limiting factor values for light, temperature, nitrogen,  
196 and silicate are written to a text file every model timestep. These are calculated by Icepack biogeochemistry, according to  
197 Jeffery et al. (2016), but there is no writing-output option in the standard code.

### 198 2.3 Model simulations

199 [Simulations were run for a refrozen lead \(RL\) without snow cover and for second-year sea ice \(SYI\) with ~40 cm snow cover](#)  
200 [monitored in April-June during the N-ICE2015 expedition \(Granskog et al., 2018 and Fig. 1 of Duarte et al. 2017\). Details on](#)  
201 [model forcing with atmospheric and oceanographic data collected during the N-ICE2015 expedition, including citations and](#)  
202 [links to the publicly available datasets are given in Fig. 2 and section 3 of Duarte et al. \(2017\) and in the Supporting information](#)  
203 [file. These data sets include wind speed, air temperature, precipitation, and specific humidity \(Hudson et al., 2015\); incident](#)  
204 [surface short and longwave radiation \(Hudson et al., 2016\); ice temperature and salinity \(Gerland et al., 2017\); sea surface](#)  
205 [current velocity, temperature, salinity and heat fluxes from a turbulence instrument cluster \(TIC\) \(Peterson et al., 2016\); sea](#)  
206 [surface nutrient concentrations \(Assmy et al., 2016\) and sea ice biogeochemistry \(Assmy et al., 2017\). Ocean forcing is based](#)  
207 [on measurements within the surface 2 meters which provide the boundary condition for the sea ice model. Model forcing files](#)  
208 [may be found in Duarte \(2021c\).](#)

209 ~~Simulations were run for a refrozen lead (RL) without snow cover and for second-year sea ice (SYI) with 40 cm snow cover~~  
210 ~~monitored in April-June during the N-ICE2015 expedition (Granskog et al., 2018 and Fig. 1 of Duarte et al. 2017). Refrozen~~  
211 ~~lead simulations started with zero ice, whereas Second Year Ice Simulations started with initial conditions described in the~~  
212 ~~Supporting information file (Table S3).~~

213 ~~We ran simulations with the standard formulations for biogeochemical processes described in Jeffery et al. (2016) and settings~~  
214 ~~described in Duarte et al. (2017), using mushy thermodynamics, vertically resolved biogeochemistry, and including: freezing,~~  
215 ~~flushing, brine mixed length and molecular diffusion within the ice and at the interface between the ocean and the sea ice as~~  
216 ~~nutrient exchange mechanisms (Jeffery et al., 2011, 2016). We ran simulations with the standard formulations for~~  
217 ~~biogeochemical processes described in Jeffery et al. (2016) and settings described in Duarte et al. (2017), using mushy~~  
218 ~~thermodynamics, vertically resolved biogeochemistry, and including: brine drainage, freezing, flushing (Turner et al., 2013;~~  
219 ~~Jeffery et al., 2016) and molecular diffusion as nutrient and algal biomass exchange mechanisms between the ocean and sea~~  
220 ~~ice. We contrasted the above simulations against others that replaced brine molecular and mixed length diffusion of nutrients~~  
221 ~~exchange at the ice-ocean interface between the ocean and the sea ice with turbulent diffusion driven by current velocity shear~~  
222 ~~(Table 2), calculated similar to heat and momentum exchanges, and following the parameterization described in McPhee et al.~~  
223 ~~(2008) and detailed above (equations 2 - 10). This contrast provides insight into the effects of changing from molecular velocity~~  
224 ~~shear onto turbulent nutrient diffusion, on-ice algal production (mg C m<sup>-2</sup> d<sup>-1</sup>), chlorophyll standing stocks (mg Chl a m<sup>-2</sup>) and~~  
225 ~~vertical distribution of chlorophyll concentration (mg Chl a m<sup>-3</sup>) [note that CICE model output for algal biomass in mmol N~~  
226 ~~m<sup>-3</sup> was converted to mg Chl a m<sup>-3</sup> as in Duarte et al. (2017), using 2.1 mg Chl a mmol N<sup>-1</sup> and following Smith et al. (1993)].~~  
227 ~~However, due to the concurrent effects of algal biomass exchange between the ocean and ice, such a contrast is not enough to~~  
228 ~~explicitly test our hypothesis and conclude about the effects of turbulent-driven nutrient supply on ice algal nutrient limitation.~~  
229 ~~Therefore, simulations were also run contrasting molecular and turbulent nutrient diffusion the same model setups, as described~~  
230 ~~above, but restarting from similar algal standing stocks and vertical distributions within the ice and, switching off algal inputs~~  
231 ~~from the water to the ice. This was done by nullifying the variable algalN, defining the ocean surface background ice algal~~  
232 ~~concentration, in file icepack\_zbgc.F90, subroutine icepack\_init\_ocean\_bio and in the restart files. In the case of the RL~~  
233 ~~simulations that started with zero ice, first a simulation was run until the 12 May, and then the obtained ice conditions were~~  
234 ~~used to restart new simulations without algal inputs from the ocean (algalN = 0 mmol N m<sup>-3</sup>). This way, when the simulations~~  
235 ~~restarted, there was already an ice algal standing stock necessary for the modelling experiments developed herein. The SYI~~  
236 ~~simulations were, by default, “restart simulations”, beginning with observed ice physical and biogeochemical variables.~~  
237 ~~Therefore, there was already an algal standing stock in the ice from the onset (Text S1 and Table S3).~~

238 ~~McPhee et al. (2008) estimated different values for  $\alpha$ , depending on whether the sea ice is growing (highest value) or melting~~  
239 ~~(lowest value) (Table 2). When running simulations with turbulent bottom diffusion for the RL, in some cases, we used only~~  
240 ~~the minimum or the maximum values for  $\alpha$ , to allow for a more extreme contrast between molecular and turbulent diffusion~~  
241 ~~parameterizations. This was done since the former value will tend to minimize differences, whereas the latter will tend to~~  
242 ~~emphasize them. We also completed simulations for the RL and for SYI changing between the maximum and the minimum~~



243 values of  $\alpha_s$ , when ice was growing or melting, respectively, and following McPhee et al. (2008) (see Table 2 for details). This  
244 parameterization with a variable  $\alpha_s$  is likely the most realistic one, accounting for double diffusion during ice melting (McPhee  
245 et al., 2008).

246 Apart from contrasting the way bottom-ice exchanges of nutrients were calculated, some simulations contrasted different  
247 parameters related to silicate limitation (Table 2). This approach follows Duarte et al. (2017), where simulations were tuned  
248 by changing the Si:N ratio and the half saturation constant for silicate uptake because silicate limitation was leading to an  
249 underestimation of algal growth. From this exercise we were able to assess if such tuning was still necessary after implementing  
250 turbulent diffusion at the ~~ice-ocean~~ interface between the ocean and the sea ice, driven by velocity shear. Moreover, we  
251 repeated simulations with varying snow heights to further investigate the interplay between light and nutrient limitation under  
252 molecular and turbulent contrasting nutrient diffusion nutrient diffusion parameterizations (Table 2).

253 Details on model forcing with atmospheric and oceanographic data collected during the N-ICE2015 expedition, including  
254 citations and links to the publicly available datasets are given in Fig. 2 and section 3 of Duarte et al. (2017) and in the  
255 supplementary information. These data sets include: wind speed, air temperature, precipitation, and specific humidity (Hudson  
256 et al., 2015); incident surface short and longwave radiation (Hudson et al., 2016); ice temperature and salinity (Gerland et al.,  
257 2017); sea surface current velocity, temperature, salinity and heat fluxes from a turbulence instrument cluster (TIC) (Peterson  
258 et al., 2016); sea surface nutrient concentrations (Assmy et al., 2016) and sea ice biogeochemistry (Assmy et al., 2017). Model  
259 forcing files may be found in Duarte (2021c).

274

275

276 Table 2. Model simulations. Refrozen lead (RL) simulation RL\_Sim1 corresponds to RL\_Sim5 described in Duarte et al. (2017) - the simulation leading  
 277 to a best fit to the observations in that study. The remaining RL simulations 2 – 5 differ from RL\_Sim1 in using turbulent diffusion at the ~~ice-ocean~~  
 278 interface between the ocean and the sea ice for nutrients in a comparable way as it is calculated for heat and driven by velocity shear. Moreover, RL\_Sim5  
 279 differs in the concentration of ice algae in the water column that colonize the sea ice bottom (algalN) and in silicate limitation related parameters. These  
 280 changes were done iteratively to fit the model to the observations. In RL\_Sim2 and RL\_Sim3 the maximum ( $\alpha_s=0.006$ ) and the minimum ( $\alpha_s=0.006/70=8.6$   
 281  $\times 10^{-5}$ ) values recommended by McPhee et al. (2008), respectively, are used throughout the simulations, to provide extreme case scenarios for comparison  
 282 with RL\_Sim1. In RL\_Sim4,  $\alpha_s=8.6 \times 10^{-5}$  when ice is not growing and  $0.006$  otherwise, as recommended by McPhee et al. (2008), to account for double  
 283 diffusive processes during ice melting that slow down mass exchanges. The remaining RL simulations (RL\_Sim6-9) are like the previous ones (RL\_Sim1-  
 284 4, respectively), except for algalN that was set to zero  $\text{mmol N m}^{-3}$ , and all simulations were restarted with the same values for all variables. Therefore,  
 285 simulations 6 – 9 may differ only from 13 May 2015, when they were restarted. Second year ice simulation SYI\_Sim\_1 is based on Duarte et al. (2017)  
 286 SYI\_Sim4 but without algal motion. SYI\_Sim2 and SYI\_Sim3 use turbulent diffusion at the ~~ice-ocean~~ interface between the ocean and the sea ice. The  
 287 former uses a decreased half saturation constant for silicate uptake, just like SYI\_Sim1, whereas the latter uses the standard CICE value. The remaining  
 288 SYI simulations (SYI\_Sim4 and 5) are like SYI\_Sim1 and 2, except for algalN that was set to zero. Simulations SYI\_Sim1 and SYI\_Sim2 were repeated  
 289 but with different initial snow thickness of 30, 20 and 15 cm to further investigate the interplay between light and silicate limitation (see text). Modified  
 290 parameter values from one simulation to the next are marked in bold, separately for RL and SYI simulations. Modified parameters are based on literature  
 291 ranges [e.g. Brzezinski (1985) and Hegseth (1992), for ratio Si2N diatoms, Nelson and Treguer (1992), for K Sil diatoms], Urrego-Blanco et al.  
 292 (2016), for R\_snw], or on previous model calibration work (Duarte et al., 2017). Parameters values were modified in the model input file ice\_in, except for  
 293 algalN and  $\alpha_s$ , that are hard-coded.

Simulations	Modified parameters (bold types below indicate the parameter abbreviation used in Icepack)					
	Silica to nitrogen ratio in diatoms (ratio Si2N diatoms)	Half saturation constant for silicate uptake (K_Sil diatoms, mM Si)	Ice algal concentration in the water (algalN, mM N)	Boolean to define the usage of either molecular (0) or turbulent diffusion (1) (kdvn)	Interface salt/nutrient turbulent exchange coefficient ( $\alpha_s$ )	Sigma coefficient for snow grain (R_snw)
RL_Sim1	1.0	2.2	11 $\cdot 10^{-4}$	0	-	1.5
RL_Sim2	1.0	2.2	11 $\cdot 10^{-4}$	<b>1</b>	<b>0.006</b>	1.5
RL_Sim3	1.0	2.2	11 $\cdot 10^{-4}$	<b>1</b>	<b>8.6<math>\cdot 10^{-5}</math></b>	<b>1.5</b>
RL_Sim4	1.0	2.2	11 $\cdot 10^{-4}$	<b>1</b>	<b>8.6<math>\cdot 10^{-5}</math>-0.006</b>	<b>1.5</b>
RL_Sim5	<b>1.7</b>	<b>5.0</b>	<b>4<math>\cdot 10^{-4}</math></b>	<b>1</b>	<b>8.6<math>\cdot 10^{-5}</math>-0.006</b>	<b>1.5</b>
RL_Sim6-9	As RL_Sim1-RL_Sim4, respectively		0	As RL_Sim1-RL_Sim4, respectively		
SYI_Sim1	1.0	2.2	11 $\cdot 10^{-4}$	0	-	0.8
SYI_Sim2	1.0	2.2	11 $\cdot 10^{-4}$	<b>1</b>	<b>8.6<math>\cdot 10^{-5}</math>-0.006</b>	0.8

Formatted

Formatted

Formatted Table

Formatted

Formatted

Formatted

Formatted

Formatted

Formatted

Formatted

Formatted

Formatted

Formatted

Formatted

Formatted

Formatted

Formatted

Formatted

Formatted

Formatted

Formatted

Formatted

Formatted

Formatted

Formatted

Formatted

Formatted

Formatted

Formatted

Formatted

Formatted

Formatted

Formatted

<u>SYI_Sim3</u>	1.0	4.0	$11 \cdot 10^{-4}$	1	$8.6 \cdot 10^{-5} - 0.006$	0.8
<u>SYI_Sim4 and 5</u>	As SYI_Sim1 and SYI_Sim2, respectively		0	As SYI_Sim1 and SYI_Sim2, respectively		

	Name	Description
Refrozen-lead simulations	RL_Sim1	Standard CICE parameters, except for: (i) decreased Si:N ratio from 1.8 to 1.0, well within published ranges (e.g. Brzezinski, 1985; Hegseth, 1992); (ii) decreased half saturation constant for silicate uptake proportionately as the previous ratio, from 4.0 to 2.2 mM within published limits (e.g. Nelson and Treguer, 1992); (iii) decreased colonization in the same proportion as previous parameters by setting ice algal concentration in the water column (algalN) to $11 \cdot 10^{-4} \text{ mmol N m}^{-2}$ .
	RL_Sim2	As RL_Sim1 but with molecular diffusivity at the ice-ocean interface replaced with turbulent

Formatted: Font: (Default)

Formatted: Font: (Default)

Formatted: Font: (Default)

Formatted: Font: (Default)

Formatted: Font: (Default)

Formatted: Font: (Default)

Formatted Table

Formatted: Centered

Formatted: Centered

		exchanges, always using the highest value for $\alpha_s$ , as recommended by McPhee et al. (2008).
	RL_Sim3	As RL_Sim2 but always using the lowest value for $\alpha_s$ , as recommended by McPhee et al. (2008).
	RL_Sim4	As RL_Sim3 but using either the lowest value for $\alpha_s$ , as recommended by McPhee et al. (2008), when ice is not growing, or the highest one, otherwise.
	RL_Sim5	As RL_Sim4 but changing half saturation constant for silicate uptake to 5.0 mM and Si:N to 1.7. Moreover, algalN was reduced to $4 \times 10^{-4}$ mmol N m <sup>-3</sup> .
	RL_Sims6-9	As RL_Sim1-4, respectively, except for algalN that was set to zero, and all simulations were restarted with the same values for all variables in the 13 May 2015.
Second-year ice simulations	SYI_Sim1	Standard CICE parameters, except for: (i) the sigma coefficient for snow grain ( $R_{snw}$ ) (Urrego-Blanco et al., 2016) that was reduced from 1.5 to 0.8 following Duarte et al. (2017) and (ii) the decreased Si:N ratio and the reduced half saturation constant for silicate

Formatted: Centered

Formatted: Centered

Formatted: Centered

Formatted: Centered

Formatted Table

Formatted: Centered

	uptake and algalN as in RL_Sim1 above
SYI_Sim2	As SYI_Sim1 but with molecular diffusivity at the ice-ocean interface replaced with turbulent exchanges using either the lowest value for $\alpha_s$ , as recommended by McPhee et al. (2008), when ice is not growing, or the highest one, otherwise.
SYI_Sim3	As SYI_Sim2 but changing half saturation constant for silicate uptake back to CICE original value (4.0 mM).
SYI_Sim4 and 5	As SYI_Sim1 and 2, respectively, except for algalN that was set to zero.

Formatted: Centered

Formatted: Centered

Formatted: Centered

295

### 296 3. Results

297 The results of the simulations listed in Table 2 and presented below may be found in Duarte (2021d).

#### 298 3.1 Refrozen lead simulations

299 All simulations with turbulent diffusion (RL\_Sim2 – RL\_Sim5, Table 2), predict higher bottom chlorophyll *a* (*Chl a*)  
300 concentration than with the standard molecular diffusion formulation (RL\_Sim1) (Fig. 1a). Simulations RL\_Sim2 - 4 grossly  
301 overestimate observations. Simulation RL\_Sim3, using the lowest value for  $\alpha_s$ , is closer both to observations and to RL\_Sim1,  
302 as well as RL\_Sim5, with the latter having the same  $\alpha_s$  values of RL\_Sim4 but a half saturation constant for silicate limitation  
303 increased from its tuned value in Duarte et al. (2017) of 2.2  $\mu\text{M}$  to 5.0  $\mu\text{M}$  and algalN reduced (Table 2) to bring model results  
304 closer to observations. Patterns between simulations for the whole ice column and considering both standing stocks and net  
305 primary production, are similar to those observed for the bottom-ice (Fig. 1b). Algal biomass is concentrated at the bottom  
306 layers (Fig. 2). Concentrations in the layers located between the bottom and the top of the brine network (green lines in the  
307 map plots) are  $< 10 \text{ mg Chl } a \text{ m}^{-3}$ . Ice thickness, temperature and salinity profiles are extremely similar among these simulations  
308 (Figs. S1 and S2).

309 Results for the silicate and nitrogen limiting factors are based on brine concentrations. Limiting factors exhibiting lower values  
310 (more limitation) in RL simulations are silicate, followed by light (Figs. 3, S3 – S5). Limiting values for silicate range between  
311 zero (maximum limitation) and one (no limitation), with higher-stronger limitation after May 13 in all simulations (Fig. 3).  
312 The most severe silicate limitation is for RL\_Sim1, where values drop to near zero around middle May. Despite the high  
313 average bottom *Chl a* concentration predicted in all simulations the bottom layer is where silicate limitation is less severe after  
314 May 13. This is more evident in simulations with turbulent diffusion, where light limitation at the bottom-ice becomes more  
315 severe than silicate limitation around the end of May (Fig. S6).

316 Results obtained with RL\_Sim6-9, without algal exchanges between the ocean and the ice (see Table 2), show similar patterns  
317 of those observed with RL\_Sim1-5, respectively (Fig. 4 versus Fig. 2, Fig. S9 versus Fig. 3, Figs. S7 and S8 versus Figs. S1  
318 and S2, Figs. S10 – S12 versus Figs. S3 – S5).

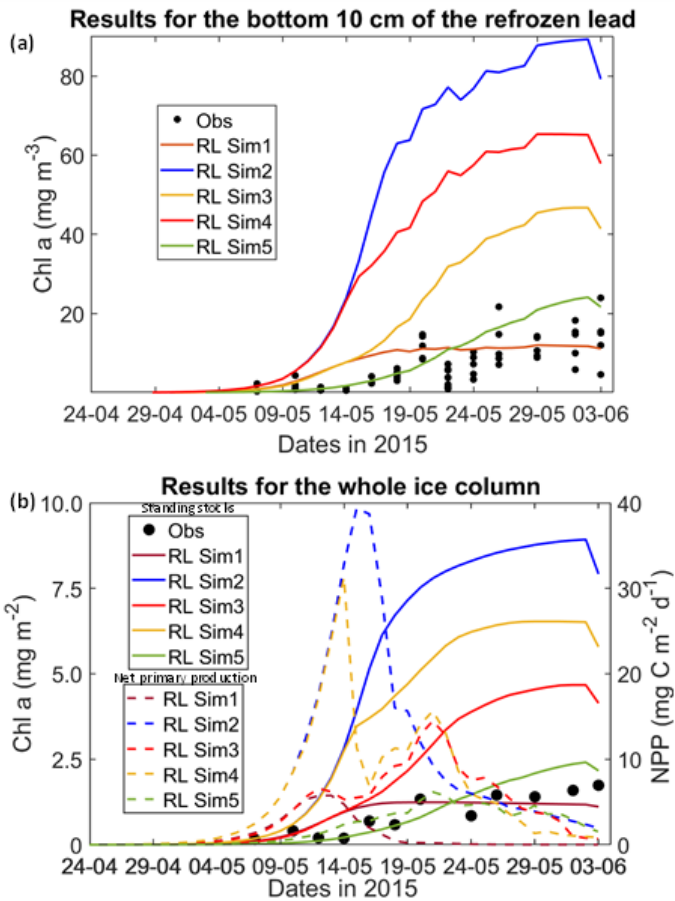
319 Interface diffusivity (one of CICE ~~tracers~~diagnostic variables, expressing corresponding to the diffusion coefficient diffusivity  
320 between adjacent biogeochemical layers and between the bottom layers and the ocean) for simulations with turbulent  
321 exchanges ( $\alpha_{it} * H$ ) are up to two orders of magnitude higher at the bottom (diffusivity between the bottom layer and the ocean)  
322 than for than for the RL\_Sim1 simulation simulations with only molecular diffusion ( $D_w$ ) or  $D_m$  + the mixed length diffusion  
323 coefficient ( $D_{MLD}$ ) (refer 2.1 and Fig. 5).

325

Formatted: Font: Italic

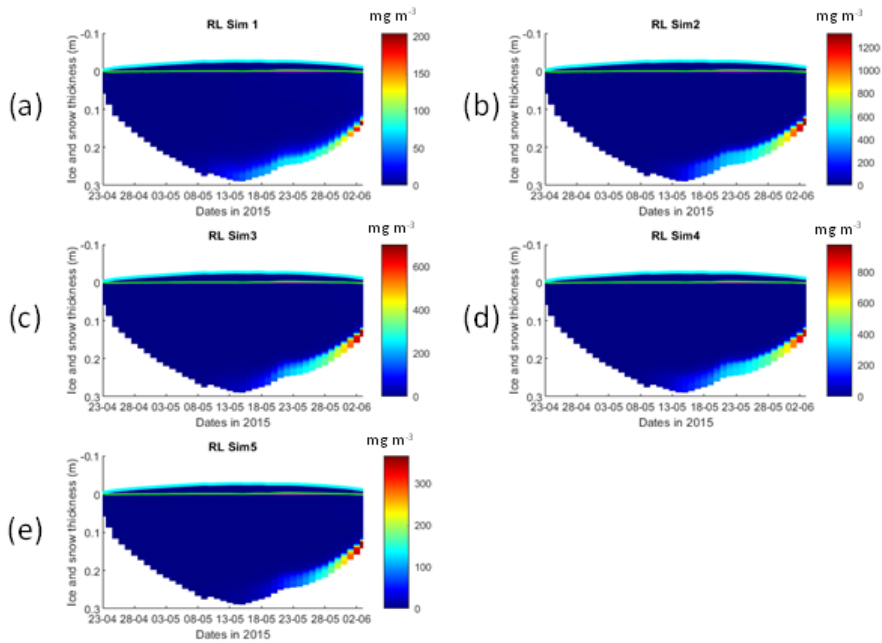
Formatted: Font: Italic, Subscript

Formatted: Font: 10 pt, Not Bold



326  
 327 **Figure 1.** Daily averaged results for the refrozen lead (RL): (a) Observed and modelled *Chl a* concentration values averaged for the  
 328 ice bottom 10 cm; (b) Observed and modelled *Chl a* standing stock (continuous lines) and modelled net primary production (NPP)  
 329 (dashed lines) for the whole ice column (refer to Table 2 for details about model simulations). Observations are the same presented  
 330 in Duarte et al. (2017).





331

332

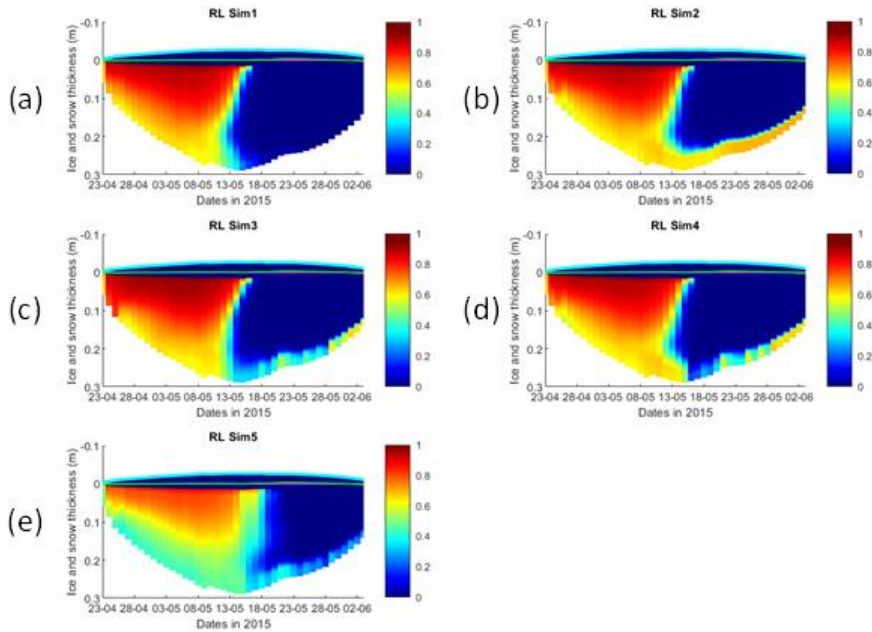
333

334

335

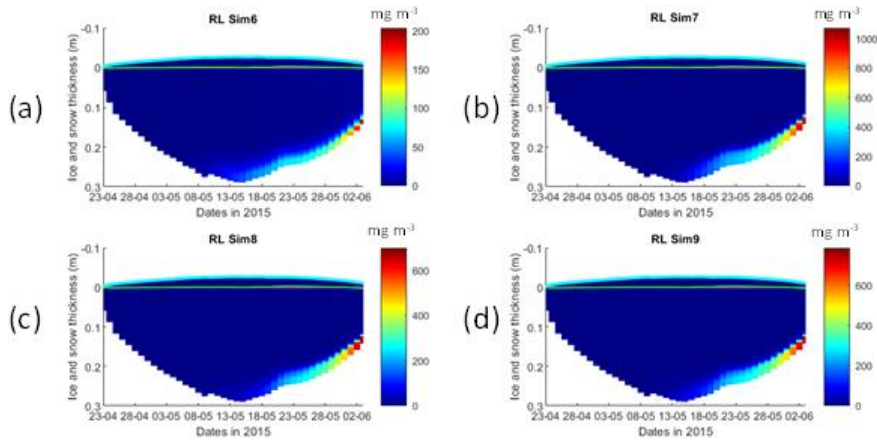
336

Figure 2. Daily averaged results for the refrozen lead (RL) simulations 1 - 5: Simulated evolution of ice algae *Chl a* as a function of time and depth in the ice (note the colour scale differences between the various panels). Ice thickness is given by the distance between the upper and the lower limits of the maps. The upper regions of the graphs, above the green line with zero values, are above the CICE biogrid and have no brine network. The magenta line, partly covered by the green line, represents sea level. Refer to Table 2 for details about model simulations.



337  
338  
339  
340  
341  
342

Figure 3. Daily averaged results for the refrozen lead (RL) simulations 1 - 5: Simulated evolution of silicate limitation (one means no limitation and zero is maximal limitation), as a function of time and depth in the ice. Ice thickness is given by the distance between the upper and the lower limits of the maps. The upper regions of the graphs, above the green line with zero values, are above the CICE biogrid and have no brine network. The magenta line, partly covered by the green line, represents sea level. Refer to Table 2 for details about model simulations.



343

344

345

346

347

348

Figure 4. Daily averaged results for the refrozen lead (RL) simulations 6 - 9: Simulated evolution of ice algae *Chl a* as a function of time and depth in the ice (note the colour scale differences between the various panels). Ice thickness is given by the distance between the upper and the lower limits of the maps. The upper regions of the graphs, above the green line with zero values, are above the CICE biogrid and have no brine network. The magenta line, partly covered by the green line, represents sea level. Refer to Table 2 for details about model simulations.

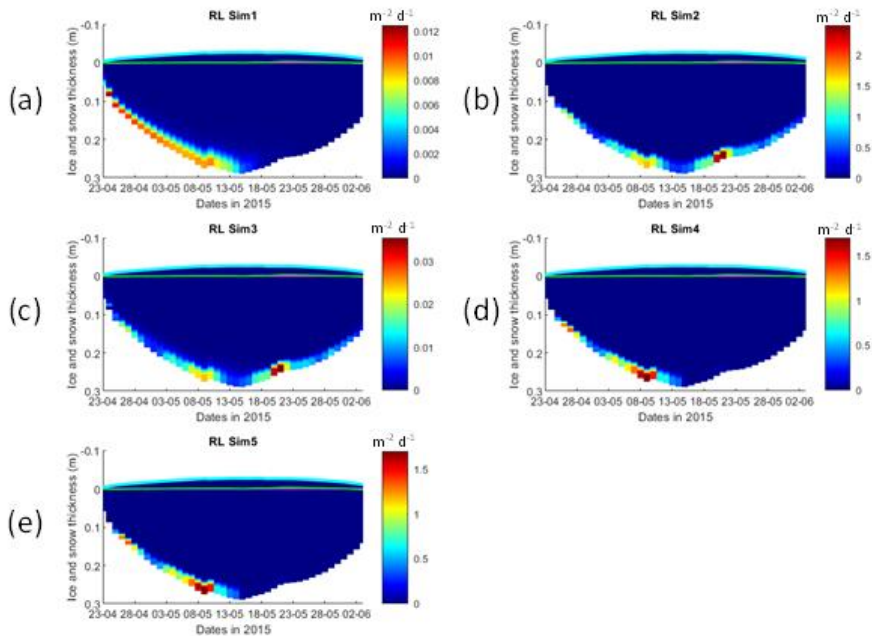


Figure 5. Daily averaged results for the refrozen lead (RL) simulations 1-5: Simulated evolution of interface diffusivity as a function of time and depth in the ice (note the colour scale differences between the various panels). In (a) interface diffusivity corresponds only to the molecular diffusion coefficient ( $D_w$ ) or to  $D_w +$  the mixed length diffusion coefficient ( $D_{MLD}$ ). In the remaining panels and at the bottom layer it corresponds to the turbulent diffusion coefficient ( $\alpha_w h$ ) (refer 2.1). Ice thickness is given by the distance between the upper and the lower limits of the maps. The upper regions of the graphs, above the green line with zero values, are above the CICE biogrid and have no brine network. The magenta line, partly covered by the green line, represents sea level. Refer to Table 2 for details about model simulations.

### 3.2 Second year ice simulations

Simulations with turbulent diffusion (SYI\_Sim2 and 3), predict only slightly higher standing stocks and net primary production than with the standard molecular diffusion formulation (SYI\_Sim1) (Fig. 6). The visual fit to the standing stock observations is comparable between the various simulations. Changing the half saturation constant for silicate limitation from 2.2 to 4.0  $\mu\text{M}$  has no impact on model results. This is confirmed by analysing the evolution of *Chl a* concentration as a function of time and depth in the ice (Fig. 7), with only minor differences being apparent towards the end of the simulation, when *Chl a* increases

Formatted: Font: Italic

Formatted: Font: Italic, Subscript

Formatted: Font: Italic

Formatted: Font: Italic, Subscript

Formatted: Font: Bold

Formatted: Font: Bold

Formatted: Font: 9 pt, Bold

364 at the bottom layers in the simulations with turbulent diffusion (SYI\_Sim 2 and 3). Ice thickness, temperature and salinity  
365 profiles are extremely similar among these simulations (Fig. S13).

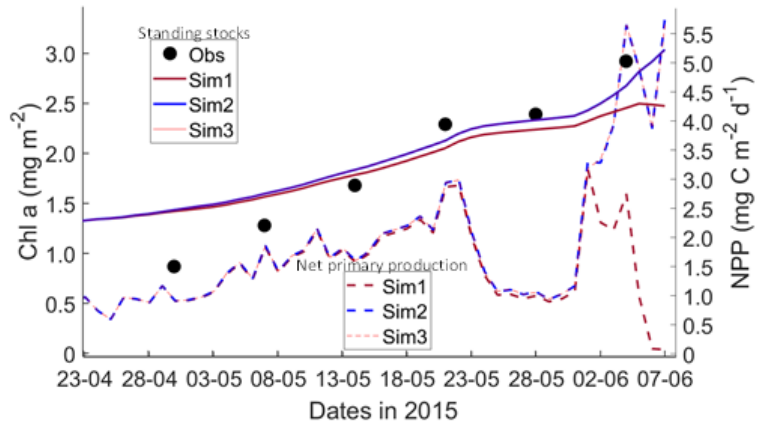
366 The dominant limiting factor in these simulations is light, ~~seconded-followed~~ by silicate (compare Fig. 8a, c and e with 8b, d  
367 and f and with Fig. S14). Light limitation is less severe after the onset of snow and ice melting at the beginning of June. Silicate  
368 limitation is very strong above the bottom ice. Nitrogen limitation is highest at a depth range between ~0.4 ~0.7 m below the  
369 ice top, with a large overlap with the depth range where a *Chl a* maximum is observed (Fig. 7). ~~Maximal *Chl a* concentration  
370 predicted for the RL\_Sim1 and RL\_Sim5 simulations - those closer to observations - are two orders of magnitude higher than  
371 those predicted for SYI (Fig. 2a and e versus Fig. 7). However, standing stocks predicted for RL\_Sim1 and RL\_Sim5  
372 simulations are smaller than for SYI simulations, as confirmed by the observations (Figs. 1b and 6). Maximum *Chl a* values  
373 predicted for SYI are between two and three orders of magnitude lower than those predicted for the RL (Figs. 2 and 7).  
374 However, standing stocks for the former are larger than those for the latter, considering both observational and model data  
375 (Figs. 1b and 6).~~ Opposite to what was described for the RL simulations, silicate limitation becomes more severe than light  
376 limitation at the bottom layer only in SYI\_Sim\_1, at the beginning of June, close to the end of the simulation (Fig. S15).

377 Results obtained without algal exchanges between the ocean and the ice (SYI\_Sim4 and 5, see Table 2), show the same patterns  
378 of those observed with SYI\_Sim1 and 2, respectively (Fig. 9 versus Fig. 7, Fig. S17 versus Fig. 8, Figs. S18 versus S14a - d  
379 and Figs. S16 versus S13a - d).

380 Interface diffusivity (~~one of CICE tracers~~ ~~one of CICE diagnostic variables, see above~~) for simulations with turbulent exchanges  
381 are up to four orders of magnitude higher at the bottom ice than for simulations with only molecular diffusion (Fig. S19,  
382 showing a comparison between SYI\_Sim1 and SYI\_Sim2).

383 SYI\_Sim1 and 2 were repeated with varying snow thickness (Table 2 and Figs. 10 and 11). In the former simulation (Fig. 10a),  
384 as snow height decreases, there is a reduction in light limitation and a sharp increase in silicate limitation, overtaking light  
385 limitation (values becoming lower) as early as mid-May. In the latter simulation (Fig. 10b), light limitation prevails irrespective  
386 of snow height, except in the case of the lower snow height of 15 cm where silicate becomes more limiting towards the end of  
387 the simulation. With the decrease in snow height, there is an increase in *Chl a* concentration in all simulations. Highest values  
388 for SYI\_Sim2 are ~one order of magnitude larger than those for SYI\_Sim1. Moreover, the decrease in snow heights is followed  
389 by an earlier and more intense bottom ice algal bloom.

Formatted: Font: Italic



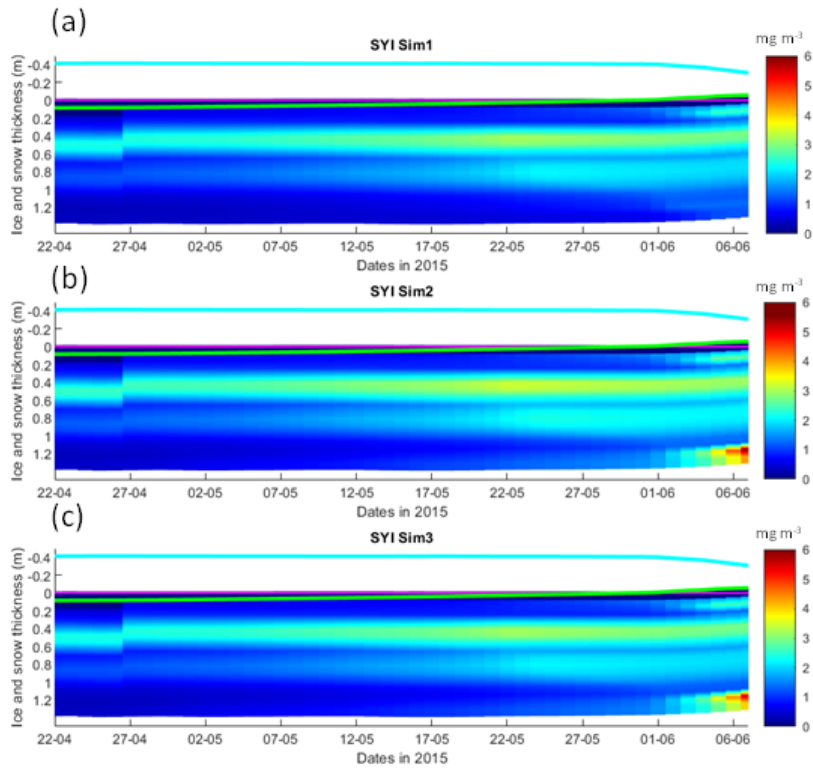
390

391

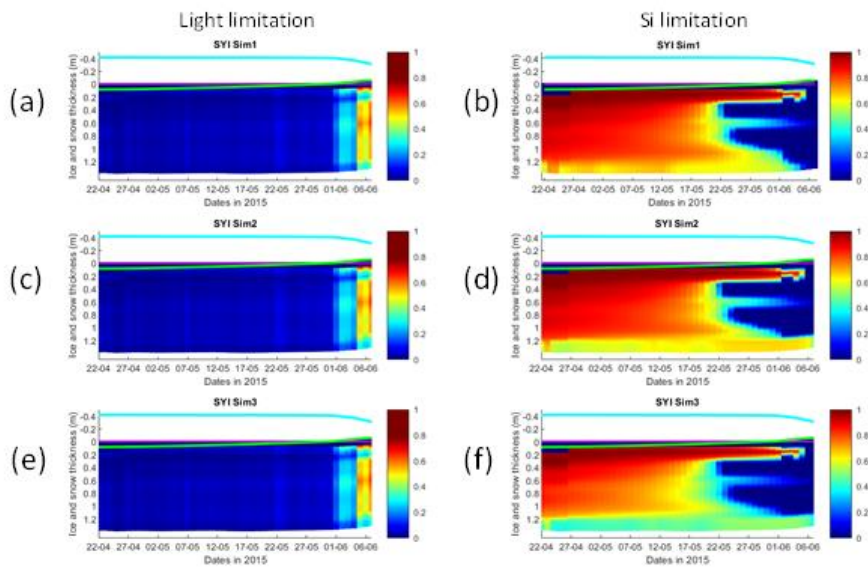
392

393

Figure 6. Daily averaged results for second year ice (SYI) simulations 1 - 3: Observed [same data presented in Duarte et al. (2017)] and modelled *Chl a* standing stock (continuous lines) and modelled net primary production (NPP) (dashed lines) for the whole ice column (refer to Table 2 for details about model simulations).



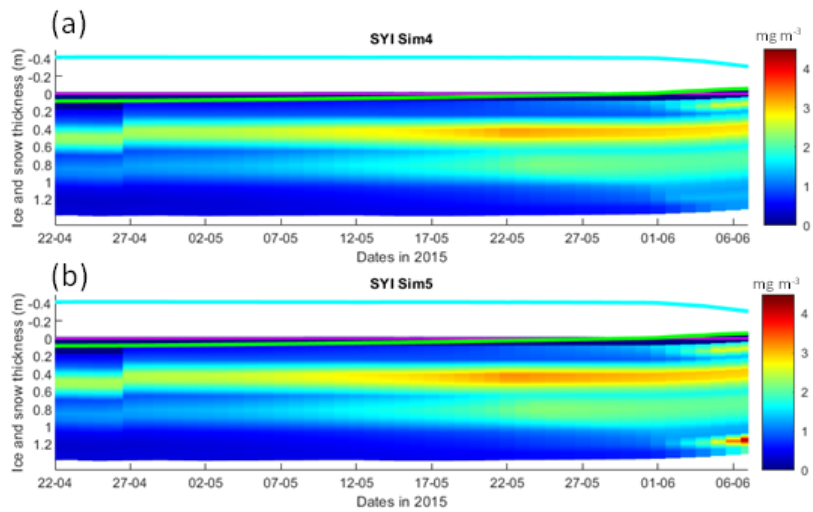
394  
 395 **Figure 7.** Daily averaged results for second year ice (SYI) simulations 1 - 3: Simulated evolution of ice algae *Chl a* as a function of  
 396 time and depth in the ice. The upper regions of the graphs, above the green line with zero values, are above the CICE biogrid and  
 397 have no brine network. The magenta line represents sea level, and the cyan line represents the top of the snow layer. Refer to Table  
 398 2 for details about model simulations.



399

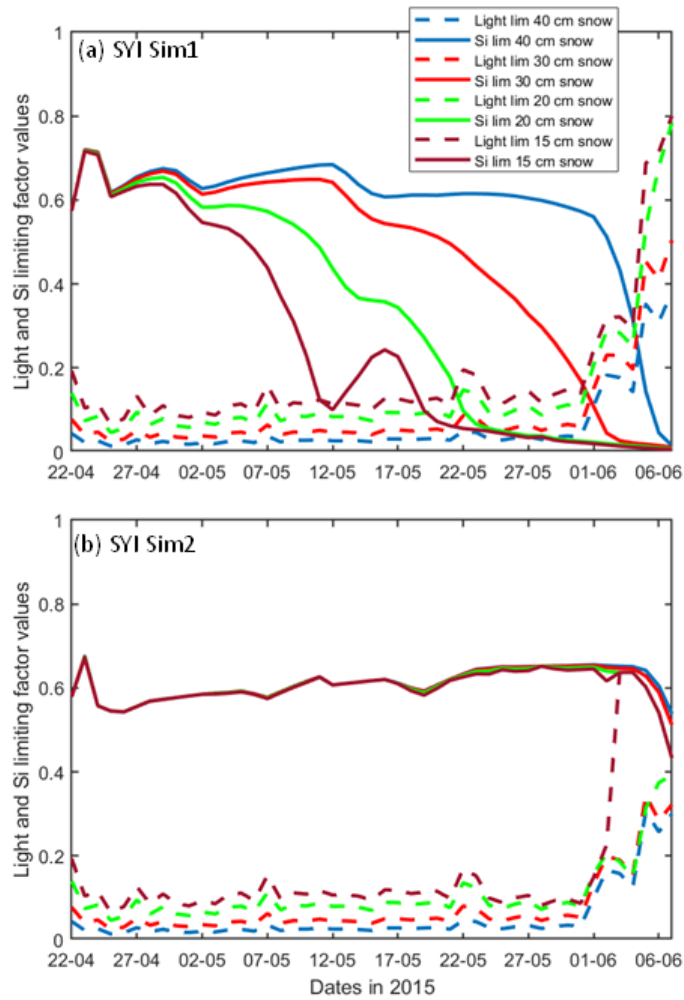
400 **Figure 8.** Daily averaged results for second year ice (SYI) simulations 1 - 3: Simulated evolution of light (left panels) and silicate  
 401 (right panels) limitation (one means no limitation and zero is maximal limitation), as a function of time and depth in the ice. The  
 402 upper regions of the graphs, above the green line with zero values, are above the CICE biogrid and have no brine network. The  
 403 magenta line represents sea level, and the cyan line represents the top of the snow layer. Refer to Table 2 for details about model  
 404 simulations.





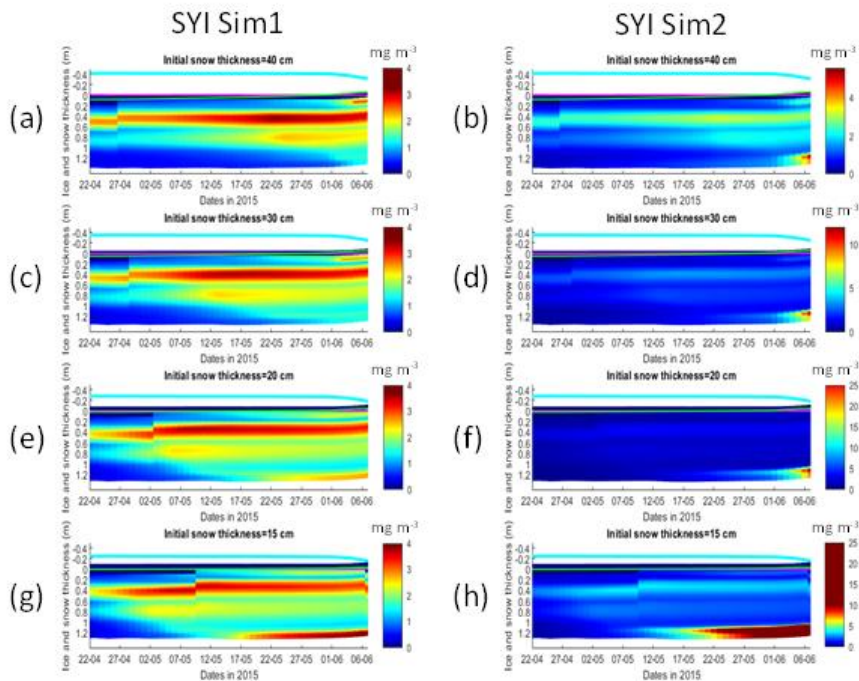
405  
406  
407  
408  
409

Figure 9. Daily averaged results for second year ice (SYI) simulations 4 and 5: Simulated evolution of ice algae *Chl a* as a function of time and depth in the ice. The upper regions of the graphs, above the green line with zero values, are above the CICE biogrid and have no brine network. The magenta line represents sea level, and the cyan line represents the top of the snow layer. Refer to Table 2 for details about model simulations.



410

411 **Figure 10.** Daily averaged results for the second-year ice (SYI) simulations 1 (a) and 2 (b) starting with a snow depth of 40 (default  
 412 simulation), 30, 20 and 15 cm: Simulated evolution of light (dashed lines) and silicate (continuous lines) limitation (one means no  
 413 limitation and zero is maximal limitation), as a function of time at the ice bottom layer (one means no limitation). Refer to Table 2  
 414 for details about model simulations.



415

416 **Figure 11.** Daily averaged results for second year ice (SYI) simulations 1 (left panels) and 2 (right panels) starting with a snow depth  
 417 of 40 (default simulation), 30, 20 and 15 cm: Simulated evolution of ice algae *Chl a* as a function of time and depth in the ice. The  
 418 upper regions of the graphs, above the green line with zero values, are above the CICE biogrid and have no brine network. The  
 419 magenta line represents sea level, and the cyan line represents the top of the snow layer. Refer to Table 2 for a description of model  
 420 simulations.

421

#### 4. Discussion

422 The results obtained in this study support the initial hypothesis, showing that [considering the role of velocity shear on turbulent](#)  
 423 [nutrient exchanges replacing molecular with turbulent diffusion at between the ice-ocean interface the ocean and the sea ice,](#)  
 424 formulated in a way consistent with momentum and heat exchanges, leads to a reduction in nutrient limitation that supports a  
 425 significant increase in ice algal net primary production and *Chl a* biomass accumulation in the bottom ice layers, when  
 426 production is understood to be nutrient limited. [Therefore, our results are in line with empirical evidence provided by Cota et](#)  
 427 [al. \(1987\) and Dalman et al. \(2019\) but, to the best of our knowledge, experimental evidence from properly dedicated](#)

428 [experiments is still lacking to test our hypothesis. Moreover, our results do not imply necessarily that experiments carried out](#)  
429 [with other sea-ice models would render the same trends.](#)

430 The implementation of turbulent mixing considerably relieved silicate limitation in the RL simulations, leading to an increase  
431 [in NPP, in the duration of the algal growth period](#), in bottom *Chl a* concentration and in-ice light absorption, increasing light  
432 limitation due to shelf-shading [in the CICE model, optical ice properties are influenced by ice algal concentrations (Jeffery et  
433 al., 2016)].

434 In the N-ICE2015 biogeochemical dataset (Assmy et al., 2016), the median of dissolved inorganic nitrogen to silicate ratios in  
435 all surface and subsurface water masses, is above 1.7 (unpublished data), which is the upper limit for the nitrogen to silicate  
436 ratio for polar diatoms (e.g. Takeda, 1998; Krause et al. 2018). Therefore, it can be expected that, in the region covered by the  
437 N-ICE2015 expedition, silicate is more limiting than nitrogen for the production yields of the pennate diatoms characteristic  
438 of the bottom-ice communities [the dominant algal functional group in bottom ice, e.g. Leu et al. (2015), van Leeuwe et al.  
439 (2019)]. Elsewhere in the Arctic the opposite may be true, considering nitrate and silicate concentrations presented in Leu et  
440 al. (2015) and the number of process studies documenting such limitation [(e.g., Campbell et al. (2016)]. However, the  
441 conclusions taken here about the effects of turbulent mixing are independent of the limiting nutrient.

442 Implementing turbulent diffusion has obvious implications for model tuning. Our results for the RL show that with this  
443 formulation it was necessary to increase the half saturation constant for silicate uptake and to reduce the ocean concentration  
444 of algal nitrogen (algalN), reducing the colonization of bottom ice by ice algae, to obtain *Chl a* values comparable to those  
445 observed (RL\_Sim5). Therefore, whereas Duarte et al. (2017) had to reduce silicate limitation to improve the fit between  
446 modelled and observational data, the opposite approach was required when using turbulent diffusion [in line with results](#)  
447 [reported in Lim et al. \(2019\) for Antarctica](#). This is an example of how one can get good model results by the wrong reasons  
448 with difficult to predict consequences on model forecasts under various scenarios.

449 In the SYI case, only a minor increase in bottom *Chl a* concentration was observed towards the end of simulations SYI\_Sim\_2  
450 and SYI\_Sim\_3, when light limitation due to the thick snow cover was relieved by snow melt. Silicate limitation was not as  
451 severe as in SYI\_Sim\_1, due to greater bottom exchanges in the former simulations. The importance of snow cover in  
452 controlling ice algal phenology has been stressed before [e.g., Campbell et al. (2015), Leu et al. (2015)].

453 Duarte et al. (2017) used the delta-Eddington parameter, corresponding to the standard deviation of the snow grain size  
454 ( $R_{\text{snow}}$ ) (Urrego-Blanco et al., 2016), to tune model predicted shortwave radiation at the ice bottom. However, there was  
455 still a positive [shortwave](#) model bias in June. Therefore, our conclusion about the main limiting role of light in SYI is  
456 conservative. Moreover, in part of SYI cores sampled during the N-ICE2015 expedition, in the period covered by our  
457 simulations, with an unusually high snow thickness (~40 cm), there was no *Chl a* bottom maximum (Duarte et al., 2017; Olsen  
458 et al., 2017).

459 The dominant role of light limitation in SYI was confirmed in the simulations with reduced snow thickness and alleviated light  
460 limitation, with a bottom-ice algal *Chl a* maximum emerging earlier at snow thickness  $\leq 20$  cm. The reduction of snow heights  
461 had a much larger effect in increasing *Chl a* concentration at the bottom layer when turbulent mixing was used, due to lower

462 silicate limitation. Reducing snow height led to a relatively early shift from light to silicate limitation when we used molecular  
463 [and mixed length](#) diffusion, whereas this shift occurred only at the very end of the simulated period when we used turbulent  
464 diffusion [driven by velocity shear](#). The effects of molecular ~~versus turbulent~~[different types of](#) diffusion, upon reduction of the  
465 snow cover and the possible development of a bottom ice algal bloom, are critical aspects when simulating ice algal phenology  
466 and attempting to quantify the contribution of sympagic algae to Arctic primary production.

467 Simulated [shear-driven](#) turbulent diffusivities are up to four orders of magnitude higher than molecular [+ mixed length](#)  
468 diffusivities and the results presented herein emphasize their potential role in sea ice biogeochemistry. The number and  
469 intensity of Arctic winter storms has increased over the 1979–2016 period (Rinke et al., 2017; Graham et al., 2017) and the  
470 effect of more frequent and more intensive winter storms in the Atlantic Sector of the Arctic Ocean is a thinner, weaker, and  
471 younger snow-laden ice pack (Graham et al., 2019). Storms that occur late in the winter season, after a deep snowpack has  
472 accumulated, have the potential to promote ice growth by dynamically opening leads where new ice growth can take place.  
473 The young ice of the refrozen leads does not have time to accumulate a deep snow layer until the melting season, which could  
474 lead to light limitation of algal growth. All things considered, it can be expected that ongoing trends in the Arctic will lead to  
475 a release from light limitation in increasingly larger areas of the ice pack in late winter, which will lead to more likely nutrient  
476 limitation earlier in spring (e.g. Lannuzel et al. 2020). These effects will be further amplified under thinning of the snowpack  
477 as observed in western Arctic, and in the Beaufort and Chukchi seas, over the last decades (Webster et al., 2014). Therefore,  
478 properly parameterizing nutrient exchanges between the ice and the ocean in sea-ice biogeochemical models is of utmost  
479 importance to avoid overestimating nutrient limitation and thus underestimating sea ice algal primary production.

480 In existing sea-ice models there are “natural” differences between the way budgets for non-conservative tracers such as  
481 nutrients are closed compared to those of momentum, heat and salt, which are related to the biogeochemical sinks and sources  
482 (e.g., equation 18 in Vancoppenolle et al., 2010), but also some “inconsistencies”, related with the way their transfers between  
483 the ocean and the ice are computed. Interestingly, some models (e.g., Jin et al., 2006, 2008 and Hunke et al., 2016) apply the  
484 diffusion equation to calculate exchanges across the bottom ice not only to dissolved tracers, but also to algal cells. This is to  
485 guarantee a mechanism of ice colonization by microalgae. However, the usage of the same coefficient for dissolved and  
486 particulate components creates significant uncertainty.

487 Molecular diffusion is a slow process compared with momentum and heat turbulent exchanges. This justifies the usage of  
488 diffusion coefficients which are much higher than molecular diffusivity, as in Jin et al. (2006), using a value of  $1.0 \times 10^{-5} \text{ m}^2$   
489  $\text{s}^{-1}$ , four orders of magnitude higher than the value indicated in Mann and Lazier (2005) –  $1.5 \times 10^{-9} \text{ m}^2 \text{ s}^{-1}$  – or the  
490 parameterization of diffusivity as a function of friction velocity as in Mortenson et al. (2017). The approach proposed herein,  
491 formulating bottom-ice nutrient exchanges in a way that is consistent with momentum and heat exchanges, provides a  
492 physically sound, consistent, and easy to implement alternative.

493 **5. Conclusions**

494 ~~Considering the role of velocity shear on turbulent nutrient exchanges~~Replacing molecular with turbulent diffusion at the ice-  
495 ~~ocean~~ at the interface between the ocean and the ice in a sea-ice biogeochemical sub-model, leads to a reduction in nutrient  
496 limitation and a significant increase in ice algal net primary production and *Chl a* biomass accumulation in the bottom-ice  
497 layers, when production is nutrient limited. The results presented herein emphasize the potential role of bottom-ice nutrient  
498 exchange processes, irrespective of brine dynamics and other physical-chemical processes, in delivering nutrients to bottom-  
499 ice algal communities, and thus the importance of properly including them in sea-ice models. The relevance of this becomes  
500 even more apparent considering ongoing changes in the Arctic icescape, with a predictable decrease in light limitation as ice  
501 becomes thinner and more fractured, with an expected reduction in snow cover.

502 **Code availability**

503 The software code used in this study may be found at:  
504 <https://doi.org/10.5281/zenodo.4675097> and <https://doi.org/10.5281/zenodo.4675021>  
505 This code is in a fork derived from the CICE Consortium repository (<https://github.com/CICE-Consortium>).  
506 The Consortium's codes are open-source with a standard 3-clause BSD license and are is under the following Copyright  
507 license, available at (<https://cice-consortium-cice.readthedocs.io/en/master/intro/copyright.html>):  
508

509 **Data availability**

510 Model forcing function files may be found at: <https://doi.org/10.5281/zenodo.4672176>  
511 Results from model simulations described above, in the form of CICE daily netCDF history files iceh.\* may be found at:  
512 <http://doi.org/10.5281/zenodo.4672210>  
513 There is one directory for each simulation, and it includes besides the historical files the input file (ice\_in) with the simulation  
514 parameters.  
515

516 **Authors contribution**

517 Pedro Duarte made the software changes, designed the experiments, performed the simulations and prepared the manuscript  
518 with contributions from all co-authors.  
519 Philipp Assmy contributed to the writing of the manuscript.  
520 Karley Campbell contributed to the writing of the manuscript.  
521 Arild Sundfjord contributed to the writing of the manuscript and to funding acquisition.  
522

523 **Competing interests**

524 The authors declare that they have no conflict of interest.

525 **Acknowledgements**

526 This work has been supported by the Fram Centre Arctic Ocean flagship project “Mesoscale physical and biogeochemical  
527 modelling of the ocean and sea-ice in the Arctic Ocean” (project reference 66200), the Norwegian Metacenter for  
528 Computational Science application “NN9300K - Ecosystem modelling of the Arctic Ocean around Svalbard”, the Norwegian  
529 “Nansen Legacy” project (no. 276730) and the European Union’s Horizon 2020 research and innovation programme under  
530 grant agreement No 869154. Contributions by K Campbell are supported by the Diatom ARCTIC project  
531 (NE/R012849/1;03F0810A), part of the Changing Arctic Ocean program, jointly funded by the UKRI Natural Environment  
532 Research Council and the German Federal Ministry of Education and Research (BMBF).

533 **References**

534 Arrigo, K. R., Kremer, J. N., and Sullivan, C. W.: A Simulated Antarctic Fast Ice Ecosystem, *J. Geophys. Res.*, 98, 17, 1993.  
535 Assmy, P., Duarte, P., Dujardin, J., Fernández-Méndez, M., Fransson, A., Hodgson, R., Kauko, H., Kristiansen, S., Mundy, C.  
536 J., Olsen, L. M., Peeken, I., Sandbu, M., Wallenschus, J., Wold, A.: N-ICE2015 water column biogeochemistry [Data set],  
537 Norwegian Polar Institute, <https://doi.org/10.21334/npolar.2016.3ebb7f64>, 2017.  
538 Assmy, P., Dodd, P. A., Duarte, P., Dujardin, J., Elliott, A., Fernández-Méndez, M., Fransson, A., Granskog, M. A., Hendry,  
539 K., Hodgson, R., Kauko, H., Kristiansen, S., Leng, M. J., Meyer, A., Mundy, C. J., Olsen, L. M., Peeken, I., Sandbu, M.,  
540 Wallenschus, J., Wold, A.: N-ICE2015 sea ice biogeochemistry [Data set], Norwegian Polar Institute,  
541 <https://doi.org/10.21334/npolar.2017.d3e93b31>, 2017.  
542 Brzezinski, M. A.: The Si-C-N Ratio of Marine Diatoms - Interspecific Variability and the Effect of Some Environmental  
543 Variables, *J. Phycol.*, 21, 347-357, 1985.  
544 Campbell, K., Mundy, C. J., Barber, D. G. and Gosselin, M.: Characterizing the sea ice algae chlorophyll a–snow depth  
545 relationship over Arctic spring melt using transmitted irradiance, *J. Mar. Sys.*, 147, 76-84, doi:  
546 <https://doi.org/10.1016/j.jmarsys.2014.01.008>, 2015.  
547 Campbell, K., Mundy, C. J., Landy, J. C., Delaforge, A., Michel, C. and Rysgaard, S.: Community dynamics of bottom-ice  
548 algae in Dease Strait of the Canadian Arctic. *Prog. Oceanogr.*, 149, 27-39, doi: <http://dx.doi.org/10.1016/j.pocean.2016.10.005>,  
549 2016.  
550 Carmack, E.: Circulation and Mixing in Ice-Covered Waters, in: *The Geophysics of Sea Ice. NATO ASI Series (Series B:  
551 Physics)*, edited by Untersteiner N. Springer, Boston, MA. 641-712, [https://doi.org/10.1007/978-1-4899-5352-0\\_11](https://doi.org/10.1007/978-1-4899-5352-0_11), 1986.  
552 Cota, G. F., Prinsenber, S. J., Bennett, E. B., Loder, J. W., Lewis, M. R., Anning, J. L., Watson, N. H. F., and Harris, L. R.:  
553 Nutrient Fluxes during Extended Blooms of Arctic Ice Algae, *J. Geophys. Res.-Oceans*, 92, 1951-1962, doi:  
554 10.1029/Jc092ic02p01951, 1987.  
555 Cota, G. F., and Horne, E. P. W.: Physical Control of Arctic Ice Algal Production, *Mar. Ecol. Prog. Ser.*, 52, 111-121, doi:  
556 10.3354/meps052111, 1989.

557 Cota, G. F., and Sullivan, C. W.: Photoadaptation, Growth and Production of Bottom Ice Algae in the Antarctic, *J. Phycol.*,  
558 26, 399-411, doi: 10.1111/j.0022-3646.1990.00399.x, 1990.

559 Dalman, L. A., Else, B. G. T., Barber, D., Carmack, E., Williams, W. J., Campbell, K. , Duke, P. J., Kirillov, S., and Mundy,  
560 C. J.: Enhanced bottom-ice algal biomass across a tidal strait in the Kitikmeot Sea of the Canadian Arctic, *Elem. Sci. Anth.*, 7,  
561 doi: <https://doi.org/10.1525/elementa.361>, 2019.

562 Duarte, P., Meyer, A., Olsen, L. M., Kauko, H. M., Assmy, P., Rosel, A., Itkin, P., Hudson, S. R., Granskog, M. A., Gerland,  
563 S., Sundfjord, A., Steen, H., Hop, H., Cohen, L., Peterson, A. K., Jeffery, N., Elliott, S. M., Hunke, E. C., and Turner, A. K.:  
564 Sea ice thermohaline dynamics and biogeochemistry in the Arctic Ocean: Empirical and model results, *J. Geophys. Res.-*  
565 *Biogeosciences*, 122, 1632-1654, doi: 10.1002/2016JG003660, 2017.

566 Duarte, P.: CICE-Consortium/Icepack: Icepack with bottom drag, heat and nutrient turbulent diffusion (Version 1.1). Zenodo.  
567 <http://doi.org/10.5281/zenodo.4675021>, (2021a, April 9).

568 Duarte, P.: CICE-Consortium/CICE: CICE with bottom drag, heat and nutrient turbulent diffusion (Version 1.1). Zenodo.  
569 <http://doi.org/10.5281/zenodo.4675097>, (2021b, April 9).

570 Duarte, P.: The importance of turbulent ocean-sea ice nutrient exchanges for simulation of ice algal biomass and production  
571 with CICE6.1 and Icepack 1.2 - CICE forcing files (Version v1.0) [Data set]. Zenodo. <http://doi.org/10.5281/zenodo.4672176>,  
572 2021c.

573 Duarte, P.: The importance of turbulent ocean-sea ice nutrient exchanges for simulation of ice algal biomass and production  
574 with CICE6.1 and Icepack 1.2 - model simulations (Version v1.0) [Data set]. Zenodo. <http://doi.org/10.5281/zenodo.4672210>,  
575 2021c.

576 Gerland, S., Granskog, M. A., King, J, Rösel, A.: N-ICE2015 Ice core physics: temperature, salinity and density [Data set],  
577 Norwegian Polar Institute, <https://doi.org/10.21334/npolar.2017.c3db82e3>, 2017.

578 Gosselin, M., Legendre, L., Demers, S., and Ingram, R. G.: Responses of Sea-Ice Microalgae to Climatic and Fortnightly Tidal  
579 Energy Inputs (Manitounuk Sound, Hudson-Bay), *Can. J. Fish. Aquat. Sci.*, 42, 999-1006, doi: 10.1139/f85-125, 1985.

580 Graham, R. M., Rinke, A., Cohen, L., Hudson, S. R., Walden, V. P., Granskog, M. A., Dorn, W., Kayser, M., and Maturilli,  
581 M.: A comparison of the two Arctic atmospheric winter states observed during N-ICE2015 and SHEBA, *J. Geophys. Res.-*  
582 *Atmospheres*, 122, 5716-5737, doi: 10.1002/2016JD025475, 2017.

583 Graham, R. M., Itkin, P., Meyer, A., Sundfjord, A., Spreen, G., Smedsrud, L. H., Liston, G. E., Cheng, B., Cohen, L., Divine,  
584 D., Fer, I., Fransson, A., Gerland, S., Haapala, J., Hudson, S. R., Johansson, A. M., King, J., Merkouridi, I., Peterson, A. K.,  
585 Provost, C., Randelhoff, A., Rinke, A., Rosel, A., Sennechael, N., Walden, V., Duarte, P., Assmy, P., Steen, H., and Granskog,  
586 M. A.: Winter storms accelerate the demise of sea ice in the Atlantic sector of the Arctic Ocean, *Sci. Rep.-Uk*, 9, Artn 9222,  
587 doi: 10.1038/S41598-019-45574-5, 2019.

588 Granskog, M. A., Fer, I., Rinke, A., and Steen, H.: Atmosphere-Ice-Ocean-Ecosystem Processes in a Thinner Arctic Sea Ice  
589 Regime: The Norwegian Young Sea ICE (N-ICE2015) Expedition, *J. Geophys. Res.-Oceans*, 123, 1586-1594, doi:  
590 10.1002/2017jc013328, 2018.



591 Hegseth, E. N.: Sub-Ice Algal Assemblages of the Barents Sea - Species Composition, Chemical-Composition, and Growth-  
592 Rates, *Polar. Biol.*, 12, 485-496, 1992.

593 Hudson, S. R., Cohen, L., Walden, V.: N-ICE2015 surface meteorology [Data set], Norwegian Polar Institute,  
594 <https://doi.org/10.21334/npolar.2015.056a61d1>, 2015.

595 Hudson, S. R., Cohen, L., Walden, V.: N-ICE2015 surface broadband radiation data [Data set], Norwegian Polar Institute,  
596 <https://doi.org/10.21334/npolar.2016.a89cb766>, 2016.

597 Hunke, E. C., Lipscomb, W. H., Turner, A. K., Jeffery, N., Elliot, S.: CICE: the Los Alamos Sea Ice Model. Documentation  
598 and User's Manual Version 5.1. Los Alamos National Laboratory, USA. LA-CC-06-012, 2015.

599 Ingram, R. G., Osler, J. C., and Legendre, L.: Influence of Internal Wave-Induced Vertical Mixing on Ice Algal Production in  
600 a Highly Stratified Sound, *Estuar. Coast. Shelf. S.*, 29, 435-446, doi: 10.1016/0272-7714(89)90078-4, 1989.

601 Jeffery, N., Hunke, E. C., and Elliott, S. M.: Modeling the transport of passive tracers in sea ice, *J. Geophys. Res.-Oceans*,  
602 116, Artn C07020, doi:10.1029/2010jc006527, 2011.

603 Jeffery, N., Elliott, S., Hunke, E. C., Lipscomb, W. H., Turner, A. K.: Biogeochemistry of CICE: The Los Alamos Sea Ice  
604 Model, Documentation and User's Manual. Zbgc\_colpkg modifications to Version 5, Los Alamos National Laboratory, Los  
605 Alamos, N. M., 2016.

606 Jin, M., Deal, C. J., Wang, J., Shin, K. H., Tanaka, N., Whitedge, T. E., Lee, S. H., and Gradinger, R. R.: Controls of the  
607 landfast ice-ocean ecosystem offshore Barrow, Alaska, *Ann. Glaciol.*, 44, 9, 2006.

608 Jin, M., Deal, C., and Jia, W.: A coupled ice-ocean ecosystem model for I-D and 3-D applications in the Bering and Chukchi  
609 Seas, *Chinese Journal of Polar Science*, 19, 11, 2008.

610 Krause, J. W., Duarte, C. M., Marquez, I. A., Assmy, P., Fernandez-Mendez, M., Wiedmann, I., Wassmann, P., Kristiansen,  
611 S., and Agusti, S.: Biogenic silica production and diatom dynamics in the Svalbard region during spring, *Biogeosciences*, 15,  
612 6503-6517, doi: 10.5194/bg-15-6503-2018, 2018.

613 Lake, R. A, Lewis, E. L.: Salt rejection by sea ice during growth, *J. Geophys. Res.*, 75, 583-597, 1970.

614 Lannuzel, D., Tedesco, T., van Leeuwe, M., Campbell, K., Flores, H., Delille, B., Miller, L., Stefels, J., Assmy, P., Bowman,  
615 J., Brown, K., Castellani, G., Chierici, M., Crabeck, O., Damm, E., Else, B., Fransson, A., Fripiat, F., Geilfus, N. X., Jacques,  
616 C., Jones, E., Kaartokallio, H., Kotovitch, M., Meiners, K., Moreau, S., Nomura, D., Peeken, I., Rintala, J. M., Steiner, N.,  
617 Tison, J. L., Vancoppenolle, M., Van der Linden, F., Vichi, M. and Wongpan, P.: The future of Arctic sea-ice biogeochemistry  
618 and ice-associated ecosystems, *Nat. Clim. Change* 10(11), 983-992, doi: <https://doi.org/10.1038/s41558-020-00940-4>, 2020.

619 Lavoie, D., Denman, K., and Michel, C.: Modeling ice algal growth and decline in a seasonally ice-covered region of the  
620 Arctic (Resolute Passage, Canadian Archipelago), *J. Geophys. Res.-Oceans*, 110, Artn C11009, doi: 10.1029/2005jc002922,  
621 2005.

622 Leu, E., Mundy, C. J., Assmy, P., Campbell, K., Gabrielsen, T. M., Gosselin, M., Juul-Pedersen, T., and Gradinger, R.: Arctic  
623 spring awakening - Steering principles behind the phenology of vernal ice algal blooms, *Progr. Oceanogr.*, 139, 151-170, doi:  
624 10.1016/j.pocean.2015.07.012, 2015.

625 [Lim, S. M., Moreau, S., Vancoppenolle, M., Deman, F., Roukaerts, A., Meiners, K. M., Janssens, J., and Lannuzel, D.: Field](#)  
626 [Observations and Physical-Biogeochemical Modeling Suggest Low Silicon Affinity for Antarctic Fast Ice Diatoms, \*J Geophys\*](#)  
627 [Res-Oceans, 124, 7837-7853, 10.1029/2018jc014458, 2019.](#)

628 Mann, K. H., Lazier, J. R. N.: Dynamics of Marine Ecosystems, Third Edition, Blackwell Publishing Ltd., Carlton, Victoria  
629 3053, Australia, 503p., doi:10.1002/9781118687901, 2005.

630 McPhee, M.: Air-ice-ocean interaction: Turbulent ocean boundary layer exchange processes. Springer-Verlag, New York,  
631 216p., doi: 10.1007/978-0-387-78335-2, 2008.

632 McPhee, M. G., Morison, J. H., and Nilsen, F.: Revisiting heat and salt exchange at the ice-ocean interface: Ocean flux and  
633 modeling considerations, *J. Geophys. Res.-Oceans*, 113, Artn C06014, doi: 10.1029/2007jc004383, 2008.

634 Mortenson, E., Hayashida, H., Steiner, N., Monahan, A., Blais, M., Gale, M. A., Galindo, V., Gosselin, M., Hu, X. M., Lavoie,  
635 D., and Mundy, C. J.: A model-based analysis of physical and biological controls on ice algal and pelagic primary production  
636 in Resolute Passage, *Elem. Sci. Anth.*, 5, Artn 39, doi:10.1525/Elementa.229, 2017.

637 Nelson, D. M., and Treguer, P.: Role of Silicon as a Limiting Nutrient to Antarctic Diatoms - Evidence from Kinetic-Studies  
638 in the Ross Sea Ice-Edge Zone, *Mar. Ecol. Prog. Ser.*, 80, 255-264, doi: 10.3354/meps080255, 1992.

639 Niedrauer, T. M., and Martin, S.: Experimental-Study of Brine Drainage and Convection in Young Sea Ice, *J. Geophys. Res.-*  
640 *Oceans*, 84, 1176-1186, doi: 10.1029/JC084iC03p01176, 1979.

641 [Notz, D., and Worster, M. G.: Desalination processes of sea ice revisited, \*J Geophys Res-Oceans\*, 114, Artn C05006, doi:](#)  
642 [10.1029/2008jc004885, 2009.](#)

643 Olsen, L. M., Laney, S. R., Duarte, P., Kauko, H. M., Fernández-Méndez, M., Mundy, C. J., Rösel, A., Meyer, A., Itkin, P.,  
644 Cohen, L., Peeken, I., Tatarek, A., Róžańska, M., Wiktor, J., Taskjelle, T., Pavlov, A. K., Hudson, S. R., Granskog, M. A.,  
645 Hop, H., and Assmy, P.: The seeding of ice-algal blooms in Arctic pack ice: the multiyear ice seed repository hypothesis, *J*  
646 *Geophys Res-Biogeosciences*, 122(7), 1529-1548, doi: 10.1002/2016jg003668, 2017.

647 [Olsen, L. M., Duarte, P., Peralta-Ferri, C., Kauko, H. M., Johansson, M., Peeken, I., Róžańska-Pluta, M., Tatarek, A., Wiktor,](#)  
648 [J., Fernández-Méndez, M., Wagner, P. M., Pavlov, A. K., Hop, H., and Assmy, P.: A red tide in the pack ice of the Arctic](#)  
649 [Ocean, \*Sci Rep\*, 9, 9536, 10.1038/s41598-019-45935-0, 2019.](#)

650 Peterson, A. K., Fer, I., Randelhoff, A., Meyer, A., Håvik, L., Smedsrud, L. H., Onarheim, L., Muilwijk, M., Sundfjord, A.,  
651 McPhee, M. G.: N-ICE2015 Ocean turbulent fluxes from under-ice turbulence cluster (TIC) [Data set], Norwegian Polar  
652 Institute, <https://doi.org/10.21334/npolar.2016.ab29f1e2>, 2016.

653 Reeburgh, W. S.: Fluxes Associated with Brine Motion in Growing Sea Ice, *Polar Biol.*, 3, 29-33, doi: 10.1007/Bf00265564,  
654 1984.

655 Rinke, A., Maturilli, M., Graham, R. M., Matthes, H., Handorf, D., Cohen, L., Hudson, S. R., and Moore, J. C.: Extreme  
656 cyclone events in the Arctic: Wintertime variability and trends, *Environ. Res. Letters*, 12, Artn 094006, doi:10.1088/1748-  
657 9326/Aa7def, 2017.

658 Smith, R. E. H., Cavaletto, J. F., Eadie, B. J., and Gardner, W. S.: Growth and Lipid-Composition of High Arctic Ice Algae  
659 during the Spring Bloom at Resolute, Northwest-Territories, Canada, *Mar. Ecol. Prog. Ser.*, 97, 19-29, doi:  
660 10.3354/meps097019, 1993.

661 Takeda, S.: Influence of iron availability on nutrient consumption ratio of diatoms in oceanic waters, *Nature*, 393, 774-777,  
662 doi: 10.1038/31674, 1998.

663 Tedesco, L., Vichi, M.: BFM-SI: a new implementation of the Biogeochemical Flux Model in sea ice. in: CMCC Research  
664 Papers, <http://www.cmcc.it/publications-meetings/publications/researchpapers/rp0081-ans-03-2010>,  
665 <http://hdl.handle.net/2122/5956>, 2010.

666 Tedesco, L., Vichi, M., and Scoccimarro, E.: Sea-ice algal phenology in a warmer Arctic, *Sci. Adv.*, 5, ARTN eaav4830, doi:  
667 10.1126/sciadv.aav4830, 2019.

668 ~~[Thomas, M., Vancoppenolle, M., France, J. L., Sturges, W. T., Bakker, D. C. E., Kaiser, J., and von Glasow, R.: Tracer](#)~~  
669 ~~[Measurements in Growing Sea Ice Support Convective Gravity Drainage Parameterizations, \*J Geophys Res-Oceans\*, 125,](#)~~  
670 ~~[ARTN e2019JC015791, doi: 10.1029/2019JC015791, 2020.](#)~~

671 Turner, A. K., Hunke, E. C., and Bitz, C. M.: Two modes of sea-ice gravity drainage: A parameterization for large-scale  
672 modeling, *J. Geophys. Res.-Oceans*, 118, 2279-2294, doi: 10.1002/jgrc.20171, 2013.

673 Urrego-Blanco, J. R., Urban, N. M., Hunke, E. C., Turner, A. K., and Jeffery, N.: Uncertainty quantification and global  
674 sensitivity analysis of the Los Alamos sea ice model, *J. Geophys. Res.-Oceans*, 121, 2709-2732, doi: 10.1002/2015JC011558,  
675 2016.

676 ~~[Vancoppenolle, M., C. M. Bitz, and T. Fichefet \(2007\), Summer landfast sea ice desalination at Point Barrow, Alaska:](#)~~  
677 ~~[Modeling and observations, \*J. Geophys. Res.\*, 112, C04022, doi:10.1029/2006JC003493.](#)~~

678 Vancoppenolle, M., Bitz, C. M., and Fichefet, T.: Summer landfast sea ice desalination at Point Barrow, Alaska: Modeling  
679 and observations, *J. Geophys. Res.-Oceans*, 112, Artn C04022, doi: 10.1029/2006jc003493, 2007.

680 ~~[Vancoppenolle, M., Goosse, H., de Montety, A., Fichefet, T., Tremblay, B., and Tison, J. L.: Modeling brine and nutrient](#)~~  
681 ~~[dynamics in Antarctic sea ice: The case of dissolved silica, \*J Geophys Res-Oceans\*, 115, Artn C02005, doi:](#)~~  
682 ~~[10.1029/2009jc005369, 2010.](#)~~

683 ~~[Vancoppenolle, M., Bopp, L., Madec, G., Dunne, J., Ilyina, T., Halloran, P. R., and Steiner, N.: Future Arctic Ocean primary](#)~~  
684 ~~[productivity from CMIP5 simulations: Uncertain outcome, but consistent mechanisms, \*Global Biogeochem Cy.\*, 27, 605-619,](#)~~  
685 ~~[doi: 10.1002/gbc.20055, 2013.](#)~~

686 van Leeuwe, M. A., Tedesco, L., Arrigo, K. R., Assmy, P., Campbell, K., Meiners, K. M., Rintala, J. M., Selz, V., Thomas,  
687 D. N. and Stefels, J.: Microalgal community structure and primary production in Arctic and Antarctic sea ice: A synthesis.  
688 *Elem. Sci. Anth.*, 6:4., doi: <https://doi.org/10.1525/elementa.267>, 2018.

689 Wakatsuchi, M., and Ono, N.: Measurements of Salinity and Volume of Brine Excluded from Growing Sea Ice, *J. Geophys.*  
690 *Res.-Oceans*, 88, 2943-2951, doi: 10.1029/JC088iC05p02943, 1983.

691 Webster, M. A., Rigor, I. G., Nghiem, S. V., Kurtz, N. T., Farrell, S. L., Perovich, D. K. and Sturm, M.: Interdecadal changes  
692 in snow depth on Arctic sea ice, *J. Geophys. Res.-Oceans* 119(8), 5395-5406, doi:10.1002/2014JC009985, 2014.  
693 [Wells, A. J., Wettlaufer, J. S., and Orszag, S. A.: Brine fluxes from growing sea ice. \*Geophys Res Lett.\* 38, Artn L04501, doi:  
694 \[10.1029/2010gl046288, 2011.\]\(#\)](#)  
695  
696  
697  
698  
699  
700